Council on Tall Buildings and Urban Habitat Korea

International Journal of
High-Rise Buildings
www.ctbuh-korea.org/ijhrb/index.php

International Journal of High-Rise Buildings
June 2025, Vol 14, No 2, 167-183
https://doi.org/10.21022/IJHRB.2025.14.2.167

Roles of Various Parameters on Dynamic Properties of Buildings Studied by Explainable Machine Learning (XML) Technique

Ying Gu, Qingshan Yang†, Ke Li , Kunpeng Guo, and Yukio Tamura

School of Civil Engineering, Chongqing University, Chongqing, 400044, China

Abstract Dynamic properties such as natural frequency and damping ratio are crucial parameters in simulating dynamic responses of buildings excited by seismic and wind forces. Traditional formulae for predicting these parameters include limited parameters such as building height and material type, ignoring many other influencing parameters. This paper discusses the effects of eight parameters, material type, building usage, building height, embedment length, longitudinal dimension, transverse dimension, pile length, and tip displacement, for predicting buildings' dynamic properties using a machine learning (ML) technique based on the Japanese Damping Database (2000). Moreover, this study employed an explainable machine learning (XML) to investigate the influence of these parameters. The natural frequency clearly decreases as the building height increases, with the height effect being the most dominant. While the effects of material type, embedment length, longitudinal dimension, building usage, and pile length are also observed, they are less significant. The damping ratio decreases as the building height increases. However, the influences of other parameters, such as tip displacement, building usage, longitudinal dimension, material type, embedment length, transverse dimension, and pile length, are also clearly evident.

Keywords: natural frequency, damping ratio, building parameters, machine learning, SHAP

†Corresponding author:
Qingshan Yang
E-mail:
qshyang@cqu.edu.cn

1. Introduction

Natural frequency and damping ratio are both fundamental dynamic properties of buildings. They both serve as comprehensive indicators of a building's mass and stiffness characteristics, and they are affected by the construction material, the soil condition, and so on. They both play a crucial role in responses to external excitations such as earthquakes and strong winds. However, it is not easy to accurately estimate them. Detailed structural information including non-load-bearing materials such as partitions, architectural finishings and so on are incomplete in the design stage for predicting natural frequency. Thus, it is commonly evaluated by FEM analyses considering only main-frames and empirical analyses of field data. There is no theoretical method for estimating a building's damping ratio.

Some researchers have proposed empirical formulae for predicting natural frequency and damping ratio based on a number of building parameters. For instance, Ellis (1980) put forward a simple approximation $f_1 = 46/H$ for the fundamental natural frequency for all buildings. Lagomarsino (1993) extended Ellis's model to provide a value of $f_1 = 46/H$ for S buildings, and $f_1 = 46/H$ for RC buildings. Here, 'S buildings' refers to steel buildings, and 'RC buildings' refers to reinforced concrete buildings. Tamura (2012) summarized a formulae for fundamental natural frequencies based on the Japanese Damping Database (JDDB) (Tamura, 1997, AIJ Report, 2000) as follows. For low-amplitude habitability design level,

$$f_1 = \begin{cases} \dfrac{67}{H} & \text{(RC buildings and SRC buildings)} \\ \dfrac{50}{H} & \text{(S buildings)} \end{cases} \tag{1}$$

Where, 'SRC buildings' refers to steel-encased reinforced concrete buildings.

Tamura et al. (2000) and Tamura (2012) also proposed formulae for torsional and higher translational modes' natural frequencies. Similar predictive formulae have also been proposed by Oliveira and Navarro (2010), Shi et al. (2013) and Wang et al. (2016).

In the above studies, the general form for predicting natural frequency can be expressed as Eq. (2):

$$f_1 = \alpha H^{\beta} \tag{2}$$

where f_1 is fundamental natural frequency and H is building height.

For the damping ratio, prediction formulae commonly have two or more terms. One is a frequency-dependent term and the other is an amplitude dependent term. Jeary (1986) introduced the following formula

$$\zeta_1 = 0.01 f_1 + 10^{\sqrt{D_L}/2} \frac{x_H}{H} \tag{3}$$

for the 1st translational mode damping, which is claimed to be applicable to all building types. Here, D_L indicates the building plan dimension along the vibration direction, and x_H indicates the tip displacement. Although the term 'tip displacement' is used in this paper following previous studies, it does not refer precisely to the displacement of the very top of the building, but rather to the displacement of the top floor. Tamura (2012) proposed damping predictors based on JDDB, composed of a height-dependent term, an amplitude-dependent term, and an adjusting term as follows.

$$\zeta_1 = \frac{0.65}{H} + 400\frac{x_H}{H} + 0.0029 \quad \text{(Steel buildings)} \tag{4}$$

$$\zeta_1 = \frac{0.93}{H} + 470\frac{x_H}{H} - 0.0018 \quad \text{(RC buildings)} \tag{5}$$

Where ζ_1 is the fundamental translational-mode damping ratio Lagomarsino (1993), Won (2004) and Ha et al. (2020) also summarized similar empirical formulae. All of these studies adopt the form shown in Eq. (6) for predicting damping.

$$\zeta_1 = A + B\frac{x_H}{H} \tag{6}$$

These damping predictors aim to establish a simple mapping method from a few selected factors to dynamic properties. However, some other important factors may also influence natural frequency and damping ratio. Asteris et al. (2015) demonstrated that factors like the presence of infill walls, wall stiffness, and SSI are also crucial for natural frequency prediction. Satake et al. (1997) examined the influences of foundation type and pile length on damping ratio. Suda et al. (1997) and Tamura (2012) investigated the influences of building usage and dimensions on damping ratio.

In recent years, machine learning (ML) methods have garnered considerable attention as an innovative modeling tool, primarily due to their robust capabilities in data feature extraction and effectively managing complex mapping relationships. Contrary to traditional polynomial fitting formulas, ML predictive models offer two significant advantages. Firstly, they incorporate more factors, resulting in more accurate predictions. Secondly, they emphasize the model's generalization ability of the predictive performance on unseen data rather than the fitting performance on training data. This ability enables the model to effectively reason and predict outcomes in practical scenarios, a capability that traditional regression formulae cannot achieve.

Some researchers have explored the application of ML techniques for predicting dynamic properties of buildings (Asteris et al., 2016, Asteris and Nikoo, 2019, Charalampalis et al., 2020). However, those studies only focused on the fundamental natural frequencies of RC frame structures. Moreover, none of them discussed how these parameters influence the natural frequency and damping under cooperative interaction, which can provide deeper insights into the structural behavior of buildings.

Anyway, only a few parameters could be considered in traditional empirical formulae, because a statistically insufficient number of data could not extract some special features of other influencing parameters. To overcome this difficulty, this study established multi-factor ML models for predicting fundamental natural frequencies and damping ratios. Besides, an explainable machine learning (XML) method is introduced to analyse parameter influence. Section 2 introduces JDDB, in which the data is primarily measured at low-amplitude levels. In this study, data from 205 buildings in the JDDB are utilized, including factors such as material type, building usage and foundation type, as well as measured values of dynamic properties. Section 3 introduces the theoretical background of ML and predictive ML models capable of robust generalization. The results of these models are compared with the traditional formulae proposed by Tamura et al. (2000) and Tamura (2012). Section 4 employs SHapley Additive exPlanations (SHAP) to discuss the contribution and influencing trend of each parameter on natural frequency and damping ratio. Finally, Section 5 gives some concluding remarks.

2. Japanese Damping Database (JDDB)

Data of dynamic properties of buildings and structures have been collected by the Sub-Committee on Damping (AIJ-SCD) established by the Architectural Institute of Japan (AIJ) in 1993 (Tamura et al., 1994, Tamura, 1997, 1998, Damping in Buildings, 2000). Reliable high-quality full-scale damping data of buildings and structures were collected by about 40 organizations and institutes, and additional data were collected from journals and proceedings published mainly after 1970. The AIJ-SCD then confirmed those measured values, and some data lacking reliability confirmation were excluded from the JDDB. Therefore, the dynamic properties and various pieces of building information and measurement methods contained in the JDDB can be treated as reliable and comprehensive.

Table 1 tabulates pieces of building information and dynamic properties for 137 S buildings, 43 SRC buildings and 25 RC buildings, totaling 205 buildings, contained in the JDDB. Some results of preliminary analyses of the

Table 1. Contents of the JDDB (Tamura et al, 2000)

Number of Buildings and Structures		
Steel Buildings (S)	Steel Encased Reinforced Concrete Buildings (SRC)	Reinforced Concrete Buildings (RC)
137	43	25
15.5 m ≤ H ≤ 282.3 m	11.6 m ≤ H ≤ 167.4 m	10.8 m ≤ H ≤ 129.8 m
Contained Information		
Building Information (17 items)	Material type of main frames Location Number of floors on the ground Number of floors under the ground Penthouse Height Dimension along the vibration direction Dimension normal to vibration direction Shape	Building usage Foundation type Embedment length Pile length Time of completion Experimental method Evaluation technique Amplitude
Dynamic Properties	Damping Ratio (up to 6th mode) Natural Frequency (up to 6th mode)	

JDDB have been reported by Ono et al. (1995), Satake et al. (1995, 1997a, 1997b), Suda et al. (1996, 1997), and Sasaki et al. (1997) as mentioned before.

This study specifically focuses on analyzing the fundamental natural frequencies and the damping ratios of these 205 buildings for primary vibration components: two translational components along the building axes. There is not enough torsional component data in the JDDB, so we do not discuss it here. Since the JDDB contains frequencies and damping ratios of each building through different experimental methods and evaluation techniques, totally 598 data points are used for model training and prediction: 426 for S buildings, 120 for SRC buildings and 52 for RC buildings.

3. Machine Learning (ML) Model

Machine learning encompasses various techniques, including Decision Trees (DT), Random Forests (RF), Neural Networks (NN) and others. NN excels in processing diverse forms of input vector, and is well-suited for solving complex tasks involving nonlinear regression. In this study, NN is chosen to learn mapping functions from potential parameters influencing dynamic properties. After training on a data set, a successful NN should show not only good fitting performance on the train data, but also good prediction performance on new tasks. This section describes how to establish ML models to predict natural frequency and damping ratio.

3.1. Basics of NN

Fully Connected Neural Network (FCNN) contains input, hidden and output layers (Haykin, 2009). Each neuron within these layers is fully connected to nodes from the preceding and succeeding layers. The connection behaves nonlinearly by employing a nonlinear activation function. Figure 1 illustrates a neuron in a hidden layer,

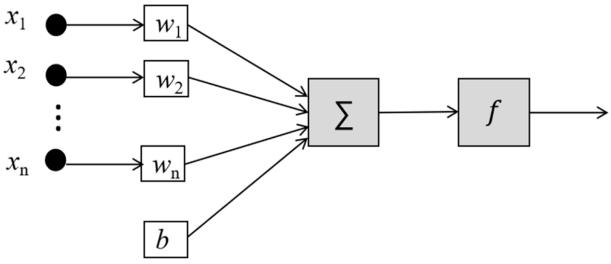


Fig. 1. A neuron with a single n-element input vector.

with an n-element input vector, and the output can be mathematically expressed as:

$$y_i = f\left(\sum_{i=1}^{n} w_i x_i + b\right) \tag{7}$$

where y_i is the output after a neuron, f denotes the activation function, w_i represents the weight of the convolution filter and b indicates the bias term.

3.2. Design of ML Models

3.2.1. Inputs and Outputs

As mentioned before, a total of 598 data points from three different material types of buildings are used. Each data set includes 17 items of building information and measured dynamic properties, as shown in Table 1. Excluding some subjective items, e.g. evaluation method, eight items are selected as parameters, and are considered as inputs in this ML model study, as depicted in Table 2 and Fig. 2. It is true that many other parameters, including structural systems, influence the natural frequency and damping ratio. However, these parameters can vary significantly and are often complex. In some cases, multiple systems are used in combination. The JDDB did not intentionally exclude such factors, but incorporating this

Table 2. Parameters used as inputs for ML models and range of input values

Parameters (Inputs)	Range of Parameter Values
Building Height: H	10 m ~ 300 m
Material Type: α	1 (S), 2 (SRC), 3 (RC)
Building Usage: β	1 (Office), 2 (Apartment), 3 (Hotel)
Longitudinal Dimension: D_L	5 m ~ 150 m
Transverse Dimension: D_T	5 m ~ 150 m
Embedment Length: L_E	0 m ~ 40 m
Pile Length: L_P	0 m ~ 80 m
Tip Displacement: x_H	0 m ~ 0.09 m

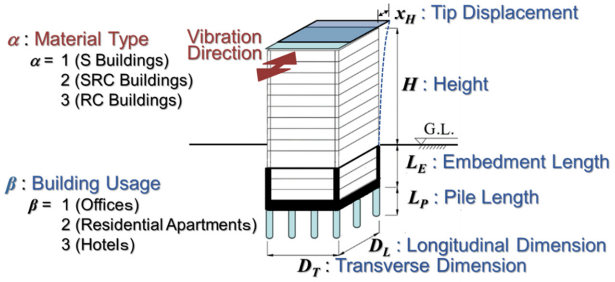


Fig. 2. Parameters examined in this paper.

detailed information proved challenging. Even if these factors were included in the JDDB, it might be difficult to distinguish their individual effects clearly. Therefore, we chose to analyze the contributions of eight representative parameters shown in Fig. 2 in this study.

In the following data preprocessing, the 598 data points are divided into three parts: training set (478 data, 80%), validation set (60 data, 10%), and testing set (60 data, 10%). These datasets are used for the subsequent model training and testing.

3.2.2. Hyperparameter Optimization

Hyperparameter tuning is necessary to find the best architecture of an ANN and to improve the performance of ML models by finding the optimal combination of hyperparameter values (Andonie, 2019).

Estimation of the best architecture avoids the overfitting problem. Overfitting is a common issue in machine learning where a model performs well on training data but poorly on validation data. This often occurs when the model is overly complex, with too many hyperparameters relative to the number of observations. To prevent overfitting, it is crucial to determine the correct number of neurons with their hidden layer.

In this study, a default architecture of 8-8-1 (8 units in the input layer, 8 units in the hidden layer and 1 unit in the output layer) for predicting dynamic properties is initially determined based mainly on the number of inputs and output parameters. The hyperparameters for NN are optimized according to the mean square error (MSE). For each model, MSE is computed for both training set and validation set and is given in Table 3. The optimum architecture is the one that gives the minimum MSE on the validation set within the lower limits of MSE value on the training set (Boger, 1997; Asteris, 2016).

$$MSE = \frac{1}{n}\sum_{i=1}^{n}(x_i - y_i)^2 \tag{8}$$

where n is the number of training data (or validation data), and x_i and y_i are the predicted and the measured values of dynamic properties.

Table 3 compares the MSE values of the default (8-8-1) and tuned ML models. It is clear that results of the tuned hyperparameter models significantly reduce errors and provide much better performance. It is worth noting the appearance of overfitting phenomenon on the 8-10-4-1 ML model and 8-12-1 ML model for damping, because they perform well on the training set but poorly on the validation set. Based on this procedure, the optimum models are an 8-12-1 ML model for the natural frequency and an 8-10-1 ML model for the damping with MSE on the validation set equal to 0.065 and 0.889, respectively.

3.3. Fitting and Predictive Performance of Models

In this study, the training set is utilized to train the model, while the validation set is used to fine-tune the model. The testing set, consisting of 60 data points, is not involved in any work. The correlation coefficient r is computed on both training and testing sets to evaluate the fitting and the final predictive performance of the optimal NNs in section 3.2.2.

$$r = \frac{\sum(x_i - \bar{x})(y_i - \bar{y})}{\sqrt{\sum(x_i - \bar{x})^2 \sum(y_i - \bar{y})^2}},\ \bar{x} = \frac{1}{n}\sum_{i=1}^{n} x_i,\ \bar{y} = \frac{1}{n}\sum_{i=1}^{n} y_i \tag{9}$$

Table 3. Comparison of MSE for different ML models

Model	Natural Frequency		Damping Ratio	
	Training Set	Validation Set	Training Set	Validation Set
8-8-1 (default model)	0.045	0.104	0.743	0.917
8-10-1	0.039	0.073	0.679	0.889
8-12-1	0.035	0.065	0.674	0.915
8-10-4-1	0.025	0.124	0.662	0.995

where n is the number of training sets (or testing sets), and x_i and y_i are the predicted and the measured values.

3.3.1. Fundamental Natural Frequency

Figure 3 illustrates the fitting performance for the training set (478 data) and the predictive performance for the testing set (60 data) of the final model. In Fig. 3(a), the correlation coefficient between the predicted and true values for the training set reaches 0.961, indicating a strong fitting ability to the known data. Figure 3(b) shows a correlation coefficient of 0.926 for the testing set, demonstrating that the model generalizes effectively to unseen data and is capable of accurately predicting a building's natural frequency.

This study primarily compares with the empirical formulae proposed by Tamura (2012), derived from the JDDB shown in Eq. (1). Then we compared S, SRC and RC buildings containing 426, 120, and 52 data points, respectively. The results of formula predictions and ML models are illustrated in Fig. 4.

These comparisons reveal that the ML models achieve higher correlation coefficients in predicting fundamental natural frequencies, as summarized in Table 4.

3.3.2. Damping Ratio

Figure 5 shows the damping ratios predicted by the ML model for the training and testing sets. By comparing

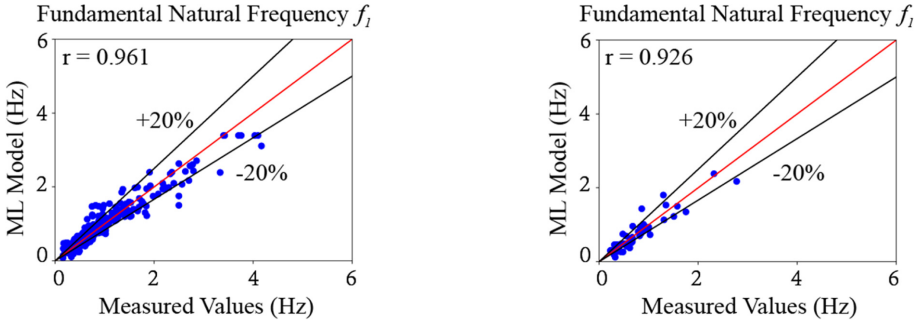
Table 4. Comparison between correlation coefficients of predicted and true values of natural Frequencies by ML models and Tamura

Material Type	ML Model	Tamura's formula (2000)
S buildings	0.963	0.942
SRC buildings	0.924	0.894
RC buildings	0.970	0.969

Figs. 5(a) and 5(b) with Fig. 3, it is found that, while the ML model performs strongly in predicting natural frequency, its performance in predicting damping ratio is less effective, which is consistent with past studies, and the ML model results show wider dispersion.

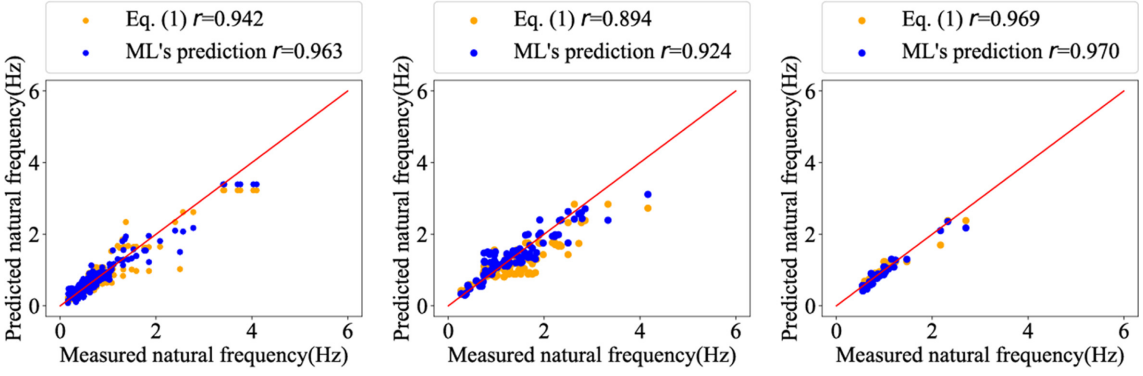
Figure 6 compares the ML model results with the damping predictors shown in Eqs. (4) and (5) (Tamura et al., 2000, Tamura, 2012). These formulae can be applied to buildings with tip drift ratio $x_H \le H \le 2 \times 10^{-5}$ and height ranges of $10\text{ m} < H < 100\text{ m}$ for RC buildings and $30\text{ m} < H < 200\text{ m}$ for S buildings (Tamura et al., 2000, Tamura 2012).

Although the damping ratio predictions show a large dispersion, the correlation coefficients by ML models for S and RC buildings are improved from 0.146 to 0.364 and from 0.716 to 0.764, respectively, compared to the empirical formulae shown in Eqs. (4) and (5). It is evident



(a) Training set (fitting ability) (b) Testing set (predictive ability)

Fig. 3. Predicted results of natural frequencies of ML model.



(a) S buildings (426 data) (b) SRC buildings (120 data) (c) RC buildings (52 data)

Fig. 4. Comparisons of natural frequencies predicted by ML models and Eq. (1) (Tamura, 2012)

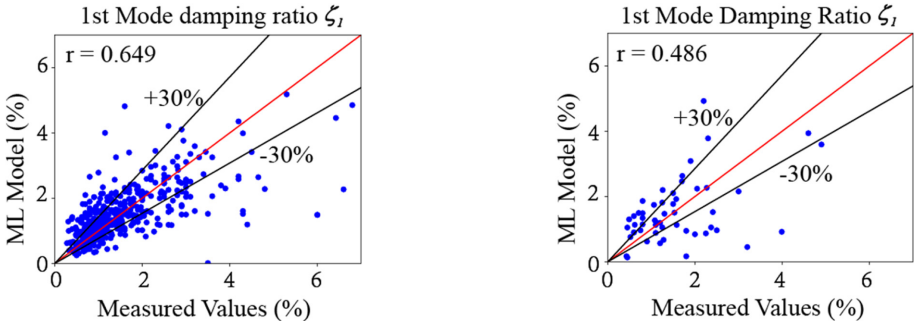


Fig. 5. Predicted results of damping ratios of ML model.

that the prediction accuracy for RC buildings is higher than that for S buildings. Tamura et al. (2000) and Tamura (2012) indicated that the damping ratios for S buildings are highly influenced by the friction damping effects at the various contact surfaces of members due to stick-slip phenomena (Aquino & Tamura, 2013a, 2013b).

4. Explainable Machine Learning (XML)

As a new branch of machine learning, explainable machine learning (XML) can help users better understand how ML models make predictions on a holistic and per-instance basis, converting opaque black-box models into transparent glass-box models. The SHapley Additive exPlanations (SHAP) chosen for this study is a kind of XML method proposed by Lundberg and Lee (2017), which describes the performance of a machine learning model (Mangalathu et al., 2020).

4.1. Basics of SHAP

SHAP is a game-theory-based approach where features are considered as players, and the act of model making predictions is analogous to playing a game (Lundberg and Lee, 2017). In this study, "features" mean eight parameters including previously chosen building dimensions. The SHAP value $f(x_j)$ of feature j is obtained by summing the mean SHAP values:

$$f(x_j)=\sum_{i=1}^{n} f(x_{ij}) \tag{10}$$

where x_i is sample i. Lundberg and Lee (2017) propose Eq. (11) to calculate $f(x_{ij})$:

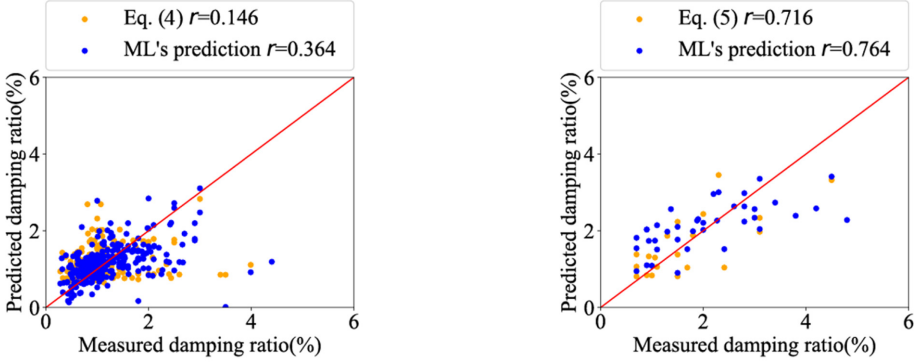
$$f(x_{ij})=\sum_{S\subseteq F\backslash\{j\}}\frac{|S|!(|F|-|S|-1)!}{|F|!}[v(S\cup\{j\})-v(S)] \tag{11}$$

where F is the set of all input features for sample x_i, $F\backslash\{j\}$ is the set of all possible combinations of features excluding feature j. $v(S)$ is the model's prediction for input sample i with features in S, and $v(S\cup\{j\})$ is the model's prediction for input sample i with features in S plus feature j.

4.2. Explanation of Fundamental Natural Frequency Prediction

In this study, the ML models for dynamic properties of buildings are examined for all data including S buildings, SRC buildings and RC buildings. Then, one ML model is made as discussed in 3.3 for the natural frequency and another for the damping ratio.

First, SHAP values for all 8 parameters are discussed in 4.2.1 Global Explanation, without separating buildings based on the main frame material types. Next, SHAP values are discussed separately for S buildings, SRC buildings, and RC buildings in 4.2.2 Local Explanation.



(a) S buildings (143 data)

(b) RC buildings (20 data)

Fig. 6. Comparison of damping ratios predicted by ML models and Eq. (4) and (5) (Tamura et al., 2000).

Here, terminologies "Global" and "Local" are used following the custom in the SHAP analysis field.

4.2.1. Global Explanation

Global explanations reveal how its inputs collectively influence the overall prediction result and laying out any relevant relationships between inputs and outputs. Here, "inputs" means values of eight parameters and "outputs" means predicted natural frequencies or damping ratios.

Figure 7(a) shows the global importance of each parameter. The abscissa shows the mean value of the absolute SHAP value across the data, and the ordinate shows eight parameters in importance order from top to bottom. It is found that building height H plays the most dominant role in predicting natural frequency with an average SHAP value of 0.42, contributing approximately 50% to the total impact. Structural-frame material a, embedment length L_E, longitudinal dimension D_L, and building use β follow it. This suggests that those parameters should be included in the estimation of natural frequency. Conversely, tip displacement x_H is the least important parameter in this SHAP analysis. The reason for the small contribution of tip displacement x_H is that most data in the JDDB include relatively small amplitude data, and the effect of tip displacement cannot be well examined. It should be noted that the amplitude dependency of the fundamental natural frequency is clear as demonstrated by Tamura et al. (1996) and Tamura (2012).

The SHAP summary plot in Fig. 7(b) illustrates the overall correlation of each parameter with the final outputs. From the figure, each parameter's correlation with the predicted natural frequency can be understood. In Fig. 7(b), parameter values are denoted by a color chart, where blue stands for lower parameter values and red for higher parameter values. A larger magnitude SHAP value means a larger contribution to the predicted natural frequency.

From the plots for building height H in Fig. 7(b), the following fact is observed. Blue plots corresponding to lower buildings lie on the positive side of the SHAP value axis. Therefore, lower buildings show a positive contribution to the predicted natural frequency, thus providing higher natural frequencies. On the other hand, red plots corresponding to higher buildings lie on the negative side of the SHAP value axis. Thus, higher buildings show a negative contribution to the predicted natural frequency and tend to give lower natural frequencies. That is, the higher the building, the lower the natural frequency. This is consistent with past studies shown by Eqs. (1) and (2).

From the plots of material type a, blue plots corresponding to $\alpha = 1$ for S buildings provide a negative contribution, whereas purple and red plots corresponding to $\alpha = 2$ and 3 for SRC and RC buildings, respectively, contribute positively. This indicates that the natural frequencies of RC buildings tend to be higher than those of S buildings. SRC buildings exhibit an intermediate feature between RC and S buildings.

4.2.2. Local Explanation

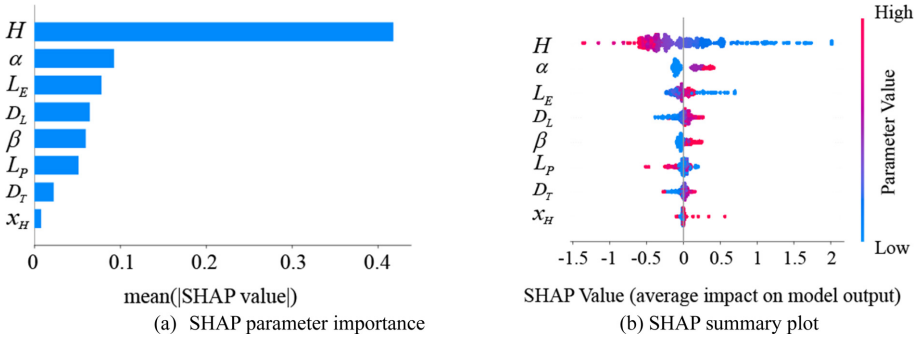
Local explanations reveal the rationale behind specific predictions on a subset of data using relevant inputs and outputs of a black-box model. The specific approach in this paper is that the parameter importance is analysed for each material type S ($\alpha = 1$), SRC ($\alpha = 2$) and RC ($\alpha = 3$) buildings separately. Therefore, the total number of parameters is seven in the following discussions.

The relation between SHAP values and parameter values is shown for seven parameters in Figs. 8, 9 and 10, for S buildings, SRC buildings and RC buildings, respectively.

In these figures, each plot corresponds to a single data set of the JDDB. The ordinate indicates SHAP values and the abscissa indicates parameter values. Positive SHAP values lead to higher natural frequency predictions, whereas negative SHAP values lead to lower natural frequency predictions. Therefore, a negative slope of the plots suggests a decreasing tendency of natural frequency with increasing parameter value, and a positive slope suggests an increasing tendency. The relationship between an individual parameter and the natural frequencies of S, SRC and RC buildings is explained later, in descending order of parameter contributions.

4.2.2.1. S buildings

(a) Building Height H: As shown in Fig. 8(a), SHAP



(a) SHAP parameter importance

(b) SHAP summary plot

Fig. 7. Global explanation for natural frequencies.

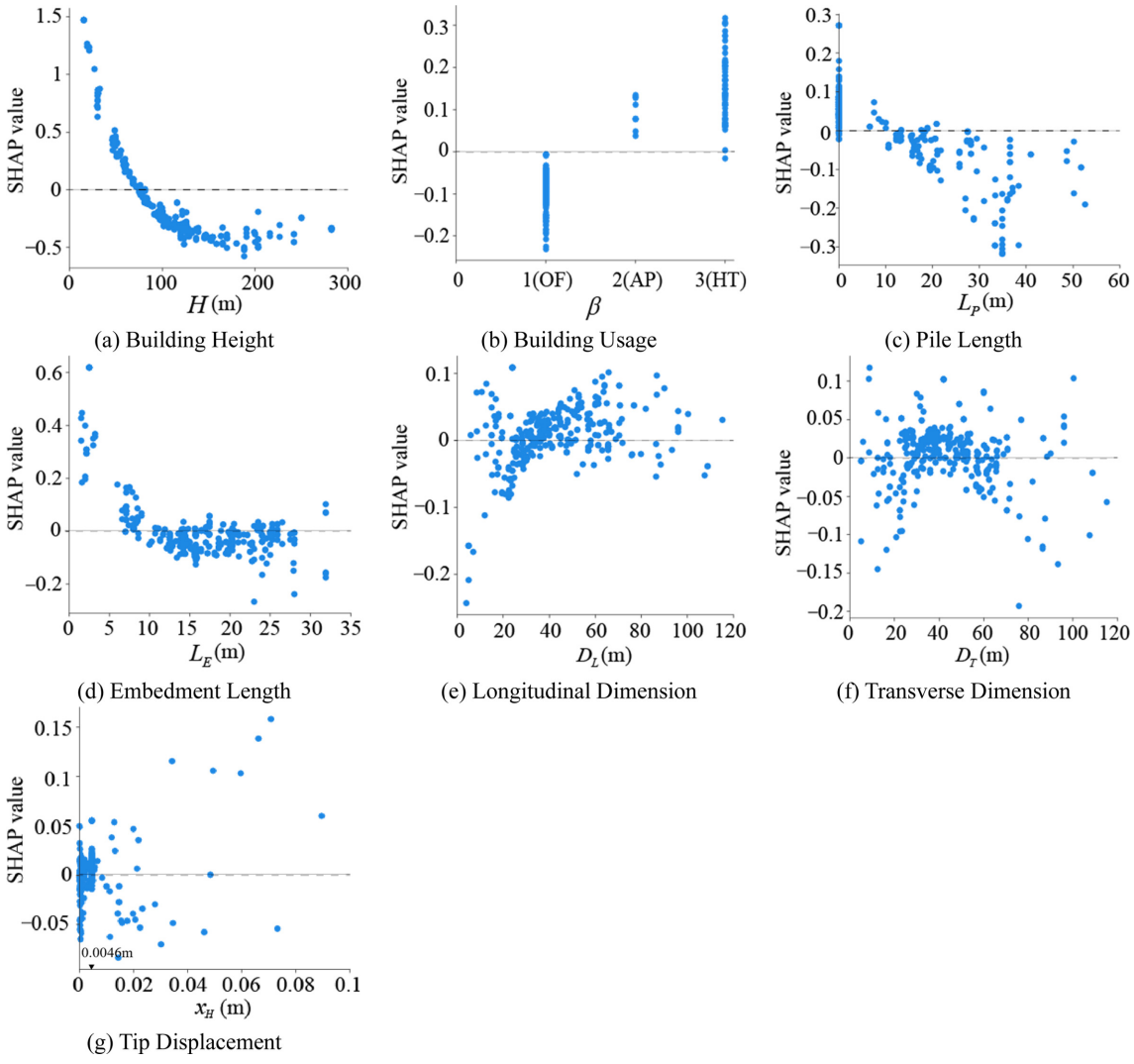


Fig. 8. Variations of SHAP values with seven parameters for natural frequencies of S buildings.

values clearly decrease with building height H, showing a negative correlation for $H < 150$ m. Thus, building height negatively influences natural frequency, i.e., the higher the building, the lower the natural frequency. It is interesting that the SHAP values almost saturate at around –0.5 for $H > 150$ m. However, as demonstrated by Satake et al. (2003), the natural period T_1 clearly increases approximately proportionally with building height H, even for heights exceeding 150 m. Since the natural frequency f_1 is inversely proportional to H, it decreases as the building height increases and approaches zero. Although it may appear to saturate at greater heights, in reality, the natural frequency may continue to decrease with increasing height.

(b) Building Usage β : As shown in Fig. 8(b), SHAP values for office buildings ($\beta = 1$) are generally negative, and give lower natural frequencies. On the other hand, SHAP values for residential apartment buildings ($\beta = 2$) and hotel buildings ($\beta = 3$) are positive, and tend to give higher natural frequencies. This might be due to the larger number of partitions and interior walls in residential apartment buildings and hotel buildings. Those non-load-bearing members also provide some stiffness in the low vibration amplitude regime as explained by the stick-slip mechanism explained by Tamura (2012) and Aquino & Tamura (2013a, 2013b). Many other parameters, including span length, can influence the natural frequency, however, there is no clear evidence regarding their effects. Conversely, Shioya et al. (1993), Tamura et al. (2000) and Tamura (2012) clearly demonstrated that the measured natural frequencies are generally more than 20% higher than the estimated natural frequency at the design stage. This discrepancy is attributed to the contribution of stiffnesses of various non-load-bearing members, including interior walls and architectural finishes. The estimated natural frequencies are based on FEM analyses, in which stiffnesses of non-load-bearing members are typically not included. Therefore, the effects of the stiffnesses of non-load-bearing elements such as partitions and interior walls can most likely be attributed to the differences in natural

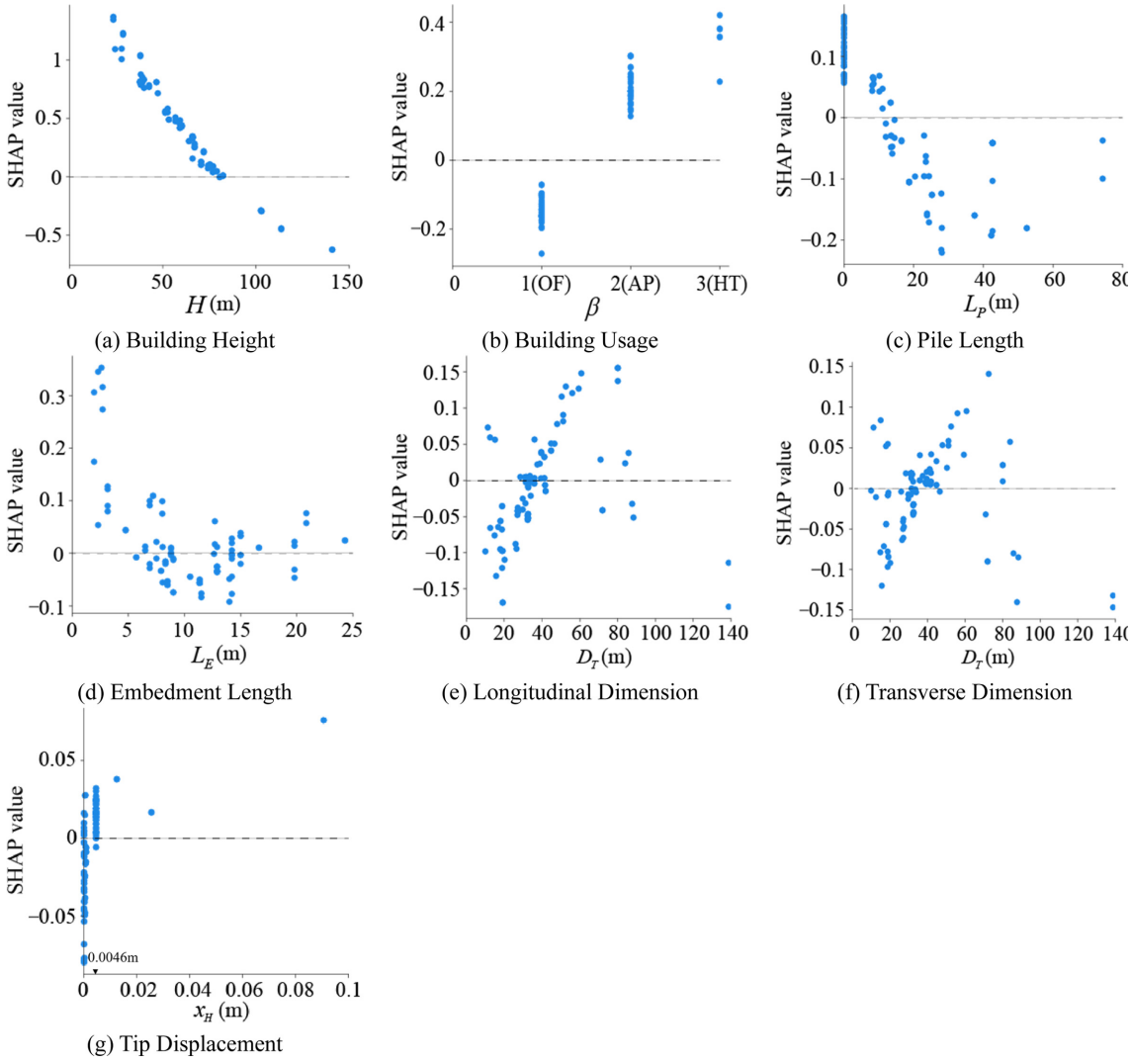


Fig. 9. Variations of SHAP values with seven parameters for natural frequencies of SRC buildings.

frequencies depending on building usage, as reported by Tamura (2012).

(c) Pile Length L_P: Pile length $L_p = 0$ means spread foundations, and they basically show positive SHAP values as shown in Fig. 8(c). Thus, buildings with spread foundations have higher natural frequencies. This is understandable, because spread foundations are generally applied in deep-embedment-length cases or hard soil conditions, so the natural frequencies tend to be higher. SHAP values generally show a negative correlation with pile length L_P up to $L_P \cong 30$ m. Thus, longer piles tend to give lower natural frequencies. It might also be understandable that a longer pile length gives similar effects as if the building height is elongated.

(d) Embedment Length L_E: As shown in Fig. 8(d), SHAP values gradually decrease with embedment length L_E, showing a clear negative correlation with embedment length for $L_E < 10$ m. Shallow embedment lengths effectively behave as if the building height has increased, due to limited soil constraints. Conversely, for deeper embedment lengths $L_E > 10$m, the SHAP values scatter below zero and don't show significant changes with increasing embedment length. This indicates that soil constraints become the dominant factor at greater embedment length, resulting in a more securely fixed building base. Consequently, further increases in embedment length do not significantly affect the natural frequency.

(e) Longitudinal Dimension D_L: As shown in Fig. 8(e), SHAP values scatter significantly, but show a slight positive correlation with longitudinal dimension as a whole. Thus, a longer longitudinal dimension D_L gives a higher natural frequency, but this is not so clear.

(f) Transverse Dimensions D_T: As shown in Fig. 8(f), SHAP values scatter significantly, and show no clear tendency.

(g) Tip Displacement x_H: As shown in Fig. 8(g), SHAP values scatter significantly, and no particular tendency can be observed. Here, many plots are located at $x_H = 0.0046$ m, which is the mean value of the amplitudes except for data with no measured amplitude. In the ML model, if data have no measured amplitude, their

amplitudes are tentatively filled with the mean value. Anyway, as most of the JDDB are low-amplitude data, no amplitude dependency can be observed in Fig. 8(g).

4.2.2.2. SRC buildings

(a) Building Height H: Like S buildings, SHAP values clearly show a negative correlation with building height as shown in Fig. 9(a). This means that higher SRC buildings have lower natural frequencies.

(b) Building Usage b: As shown in Fig. 9(b), office buildings ($\beta = 1$) show negative SHAP values, suggesting lower natural frequencies, and residential apartment buildings ($\beta = 2$) and hotel buildings ($\beta = 3$) show positive SHAP values, suggesting higher natural frequencies. Natural frequencies tend to increase in the order of office buildings, residential apartment buildings and hotel buildings, in the same way as for S buildings. This can be attributed to the effects of partitions and interior walls acting as stiffeners.

(c) Pile Length L_P: As shown in Fig. 9(c), buildings with spread foundations ($L_p = 0$) show positive SHAP values, suggesting higher natural frequencies. Thus, SHAP values show a clear negative correlation with pile length L_P for $L_P < 30$ m, suggesting that longer piles tend to give lower natural frequencies, playing a similar role to building height H. For longer pile length $L_P > 30$ m, no clear tendency can be observed. These tendencies are mostly consistent with S buildings.

(d) Embedment Length L_E: As shown in Fig. 9(d), SHAP values show a clear negative correlation with embedment length L_E for $L_E < 10$ m and saturate for $L_E > 10$ m. Thus, embedment length plays the same role as building height up to $L_E \cong 10$ m. These results are consistent with those for S buildings.

(e) Longitudinal Dimension D_L: As shown in Fig. 9(e), except for a few plots for small longitudinal dimension D_L, SHAP values show a positive correlation with longitudinal dimension D_L up to $D_L \cong 65$ m. For $D_L >$ 65 m, SHAP values likely show a negative correlation. However, as a whole, SHAP values scatter significantly,

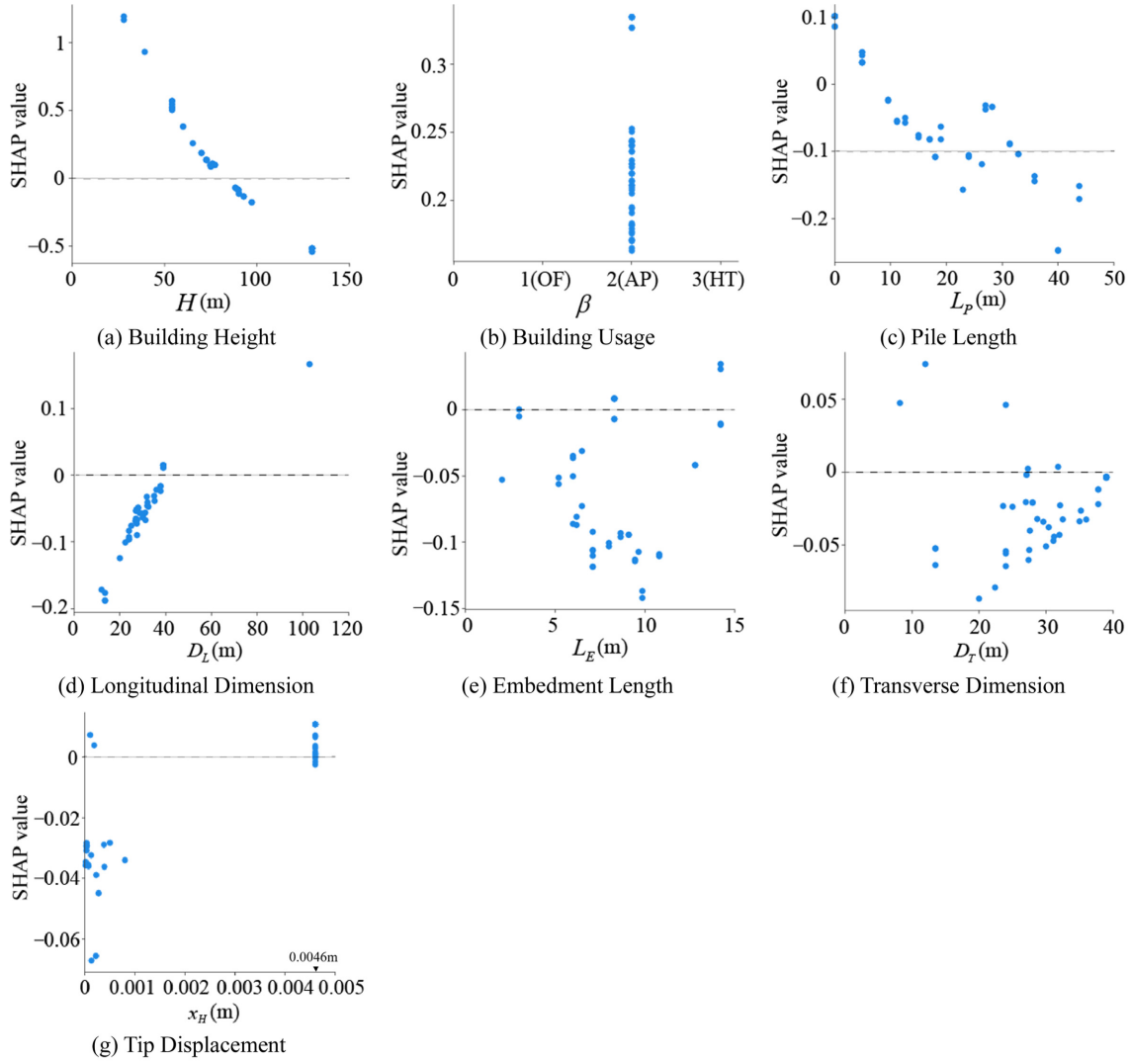


Fig. 10. Variations of SHAP values with seven parameters for natural frequencies of RC buildings.

and no clear tendency can be seen.

(f) Transverse Dimension D_T: As shown in Fig. 9(f), SHAP values distribute similar to Fig. 9(e) for longitudinal dimension D_L, showing a positive correlation with transverse dimension D_T, except for the lowest and highest ranges of D_T.

4.2.2.3. RC buildings

(a) Building Height H: As shown in Fig. 10(a), SHAP values show a very clear negative correlation with building height. It can be clearly seen that higher RC buildings have lower natural frequencies.

(b) Building Usage β: As shown in Fig. 10(b), all RC buildings contained in the JDDB are residential apartment buildings ($\beta = 2$), so the effects of building usage cannot be evaluated.

(c) Pile Length L_P: As shown in Fig. 10(c), SHAP values clearly show a negative correlation with pile length L_P. It is suggested that pile length plays a similar role to building height. A longer pile tends to give a lower natural frequency.

(d) Longitudinal Dimension D_L: As shown in Fig. 10(d), SHAP values show a clear positive correlation with longitudinal dimension D_L. Thus, a longer longitudinal dimension gives a higher natural frequency.

(e) Embedment Length L_E: As shown in Fig. 10(e), SHAP values scatter, but show a slight negative correlation with embedment length L_E for $L_E < 10$ m, in a similar manner to S and SRC buildings. This suggests that embedment length L_E plays a similar role to building height up to $L_E \cong 10$ m. For embedment length $L_E > 10$ m, SHAP values tend to show a positive correlation with embedment length L_E. However, the number of data is very limited, so no clear conclusion can be drawn.

(f) Transverse Dimension D_T: As shown in Fig. 10(f), SHAP plots seem to show a negative correlation for $D_T < 20$ m and a positive correlation for $D_T > 20$ m. However, the plots scatter significantly, so no clear conclusion can be drawn.

4.3. Explanation for Damping Ratio Prediction

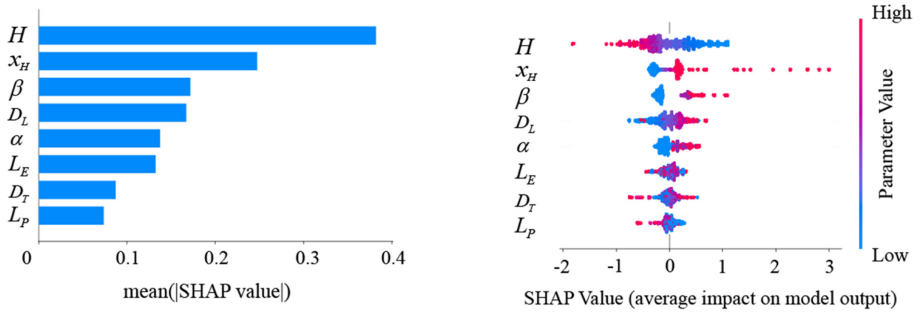
4.3.1. Global Explanation

From Fig. 11(a), it can be seen that building height H is the most important parameter affecting damping ratio, contributing approximately 30% of the variation, followed by tip displacement x_H about 18%. Past studies consistently demonstrated that these two factors have a significant impact on damping (Jeary, 1986; Lagomarsino, 1993; Tamura et al., 2000). It should be noted that the influence of parameters other than building height on the damping ratio cannot be ignored, unlike the natural frequency.

Figure 11(b) shows that building height H is negatively correlated with the SHAP value. Lower buildings, shown in blue, lie on the positive side of the SHAP axis and positively contribute to the predicted damping ratio, while higher buildings, shown in red, lie on the negative side of the SHAP axis and negatively contribute to the predicted damping ratio. Thus, lower buildings have higher damping ratios, and higher buildings have lower damping ratios. In contrast, tip displacement x_H shows a opposite tendency. Larger tip displacements, shown in red, lie on the positive side of the SHAP axis, and lower tip displacements, shown in blue, lie on the negative side of the SHAP axis. Thus, tip displacement shows a positive correlation with the predicted damping ratio, implying that higher vibration amplitudes give higher damping ratios. These facts are consistent with Tamura (2000, 2012), which demonstrated that the damping ratio usually increases with increasing amplitude in the relatively low-amplitude range. As the data contained in the JDDB are generally measured in the relatively low amplitude range, the results of this SHAP analysis are consistent with those findings.

Regarding building usage β, the blue plots for office buildings ($\beta = 1$) lie on the negative side of the SHAP axis, while the purple plots for residential apartment buildings ($\beta = 2$) and the red plots for hotel buildings ($\beta = 3$) lie on the positive side of the SHAP axis. This suggests that residential apartment buildings and hotel buildings have larger damping ratios than office buildings. This is consistent with past studies, e.g. Tamura (2012). As for the natural frequency, this can be attributed to the contributions of partitions and interior walls to the damping ratios.

Longitudinal dimension D_L is positively correlated with damping ratio, which is consistent with Jeary (1986). In



(a) SHAP parameter importance

(b) SHAP summary plot

Fig. 11. Global explanation for damping ratios.

addition, material type a is also positively correlated with damping ratio, and S buildings show lower damping ratios and SRC and RC buildings show higher damping ratios.

Embedment length L_E and transverse dimension D_T show no clear tendency.

Pile length L_P seems to be negatively correlated with the damping ratio, like the natural frequency, but this is not so clear.

4.3.2. Local Explanation

Figures 12, 13 and 14 represent the SHAP values of various parameters for S, RC and SRC buildings. The effects of each parameter on the damping ratio are discussed in descending order of the contributions of seven parameters.

4.3.2.1. S buildings

(a) Building Height H: As shown in Fig. 12(a), SHAP values show a clear negative correlation with building height. Thus, higher buildings have lower damping ratios.

(b) Building Usage β: As shown in Fig. 12(b), SHAP values for office buildings ($\beta = 1$) are negative, suggesting lower damping ratios, while SHAP values for residential apartment buildings ($\beta =$) and hotel buildings ($\beta = 3$) are positive, suggesting higher damping ratios. Like the natural frequency, this might be attributed to the effect of partitions and interior walls, which are more numerous in residential apartment buildings and hotel buildings. This result is consistent with Tamura (2012). Partitions and interior walls provide more contact surfaces producing more friction damping effects than office buildings.

(c) Longitudinal Dimension D_L: As shown in Fig. 12(c), SHAP values show a clear positive correlation with longitudinal dimension D_L, and larger longitudinal dimensions give higher damping ratios. This is consistent with the damping predictor proposed by Jeary (1986) based on records obtained for RC buildings.

(d) Tip Displacement x_H: As shown in Fig. 12(d), for small tip displacement $x_H < 0.003$ m, SHAP values show a very clear positive correlation with tip displacement.

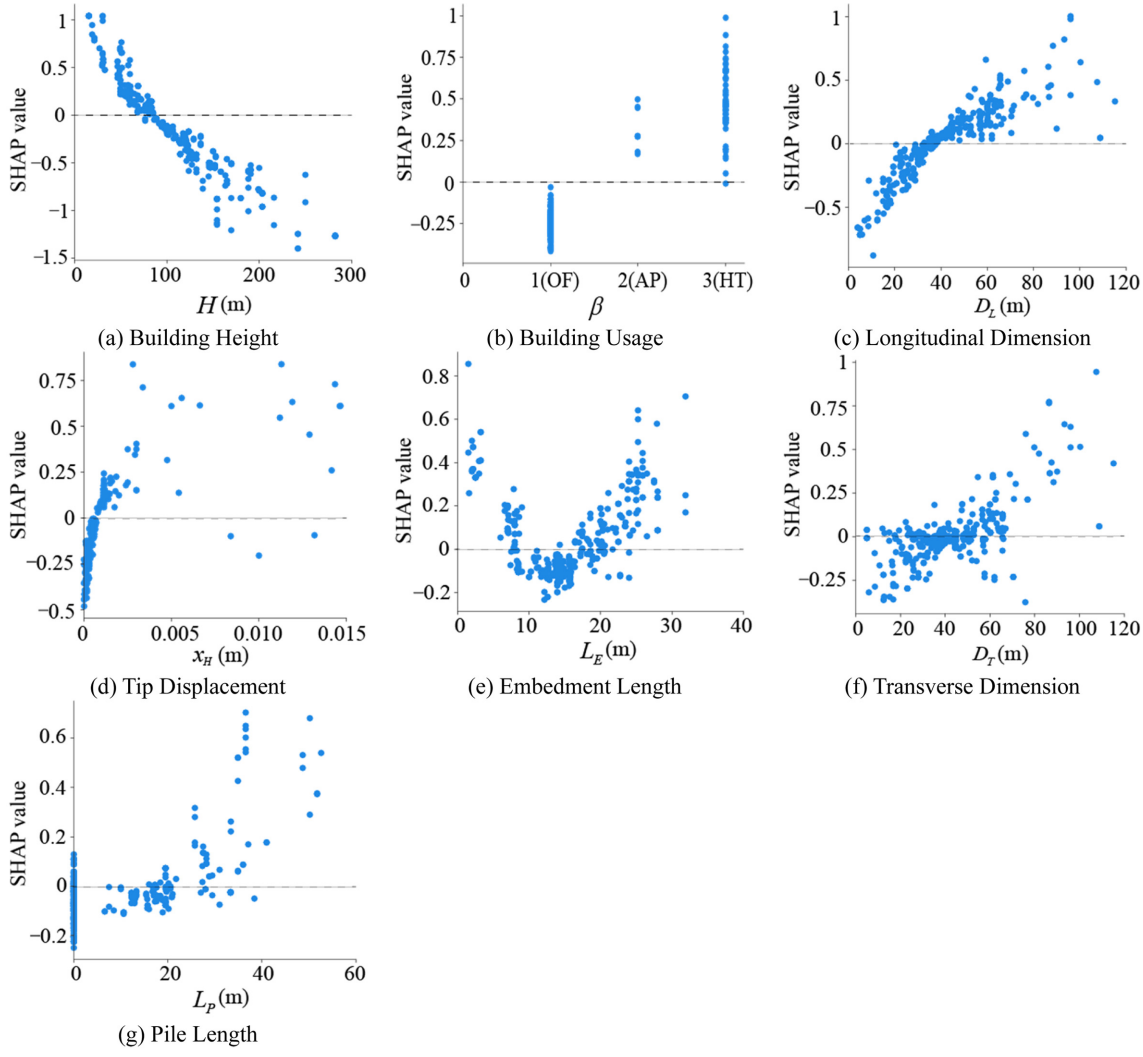


Fig. 12. Variations of SHAP values with seven parameters for damping ratios of S buildings.

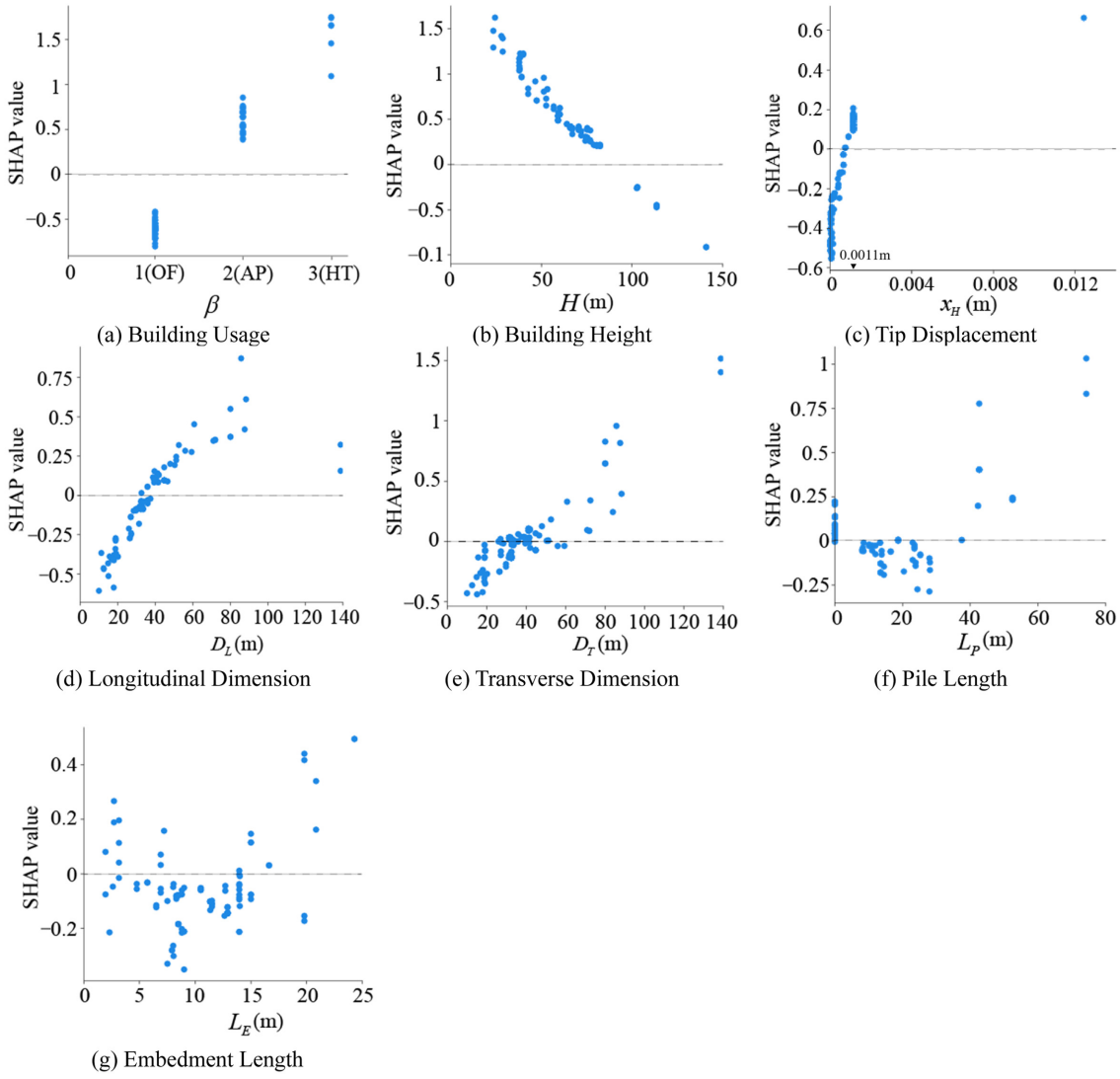


Fig. 13. Variations of SHAP values with seven parameters for damping ratios of SRC buildings.

Thus, the damping ratio increases with the amplitude. However, for large tip displacement $x_H > 0.003$ m, SHAP values are mostly positive but scatter significantly, and don't show a positive correlation with tip displacement. This suggests that the damping ratio doesn't increase with amplitude in the larger amplitude range $x_H > 0.003$ m. Tamura (2012) and Aquino & Tamura (2013a, 2013b) reported on the critical tip drift ratio, providing the maximum damping ratio. They showed four examples of large-amplitude field data, and all revealed that the damping ratio increases with amplitude up to the critical tip drift ratio $(x_H/H)_c$ and then decreases with amplitude. The critical tip drift ratios were very small: $(x_H/H)_c = 2 \times 10^{-5} \sim 10^{-4}$. Incidentally, the average height of S buildings in the JDDB is around $H_{AVE} = 107$ m, and a tip drift ratio with amplitude $x_H = 0.003$m is roughly estimated at $x_H / H = 3 \times 10^{-5}$, which is consistent with the critical tip drift ratios reported by Tamura (2012) and Aquino & Tamura (2013a, 2013b).

(e) Embedment Length L_E: As shown in Fig. 12(e), SHAP values show a negative correlation with embedment length L_E up to around $L_E \cong 10$ m, suggesting a decreasing tendency of damping ratio with embedment length, as if building height is increased. However, for deeper embedment lengths $L_E > 10$ m, SHAP values show a clear positive correlation with embedment length L_E, and the damping ratio increases with embedment length. This might be attributed to the more significant SSI effects with deeper embedment for $L_E > 10$ m.

(f) Transverse Dimension D_T: As shown in Fig. 12(f), the plots are rather scattered, but SHAP values tend to show a positive correlation with transverse dimension D_T, like the longitudinal dimensions D_L shown in Fig. 12(c). Thus, larger transverse dimensions tend to give larger damping ratios.

4.3.2.2. SRC buildings

(a) Building Usage β : Like S buildings, as shown in

Fig. 13(a), the SHAP values of office buildings ($\beta = 1$) are negative, but those of residential apartment buildings ($\beta = 2$) and hotel buildings ($\beta = 3$) are positive and increase in this order. Thus, damping ratios are lowest for office buildings, and highest for hotel buildings. This can be attributed to the contribution of partitions and interior walls.

(b) Building Height H: Like S buildings, as shown in Fig. 13(b), SHAP values show a clear negative correlation with building height H, suggesting that higher buildings have lower damping ratios.

(c) Tip Displacement x_H: As shown in Fig. 13(c), SHAP values show a clear positive correlation with tip displacement for $x_H < 0.0011$ m, suggesting that higher amplitudes give higher damping ratios.

(d) Longitudinal Dimension D_L: Like S buildings, as shown in Fig. 13(d), SHAP values show a clear positive correlation with longitudinal dimension D_L. Thus, larger longitudinal dimensions give higher damping ratios.

(e) Transverse Dimension D_T: As shown in Fig.13(e), SHAP values are clearly correlated with transverse dimension D_T in the same manner as longitudinal dimension D_L. Thus, larger transverse dimensions give higher damping ratios.

(f) Pile Length L_P: Like RC buildings, as shown in Fig. 13(f), SHAP values show a negative correlation with pile length L_P up to L_P 30m. Thus, longer pile lengths give lower damping ratios as if the building height increased, while for longer pile lengths $L_P > 30$ m, SHAP values clearly show a positive correlation, giving higher damping ratios. As mentioned before, this might be attributed to more significant SSI effects due to increasing constraints and frictions.

4.3.2.3. RC buildings

(a) Building Height H: As shown in Fig. 14(a), SHAP values show a clear negative correlation with building height H. Thus, higher buildings have lower damping ratios. This might be attributed to less SSI effects for higher buildings as pointed out by Tamura (2012).

(b) Embedment Length L_E: As shown in Fig. 14(b),

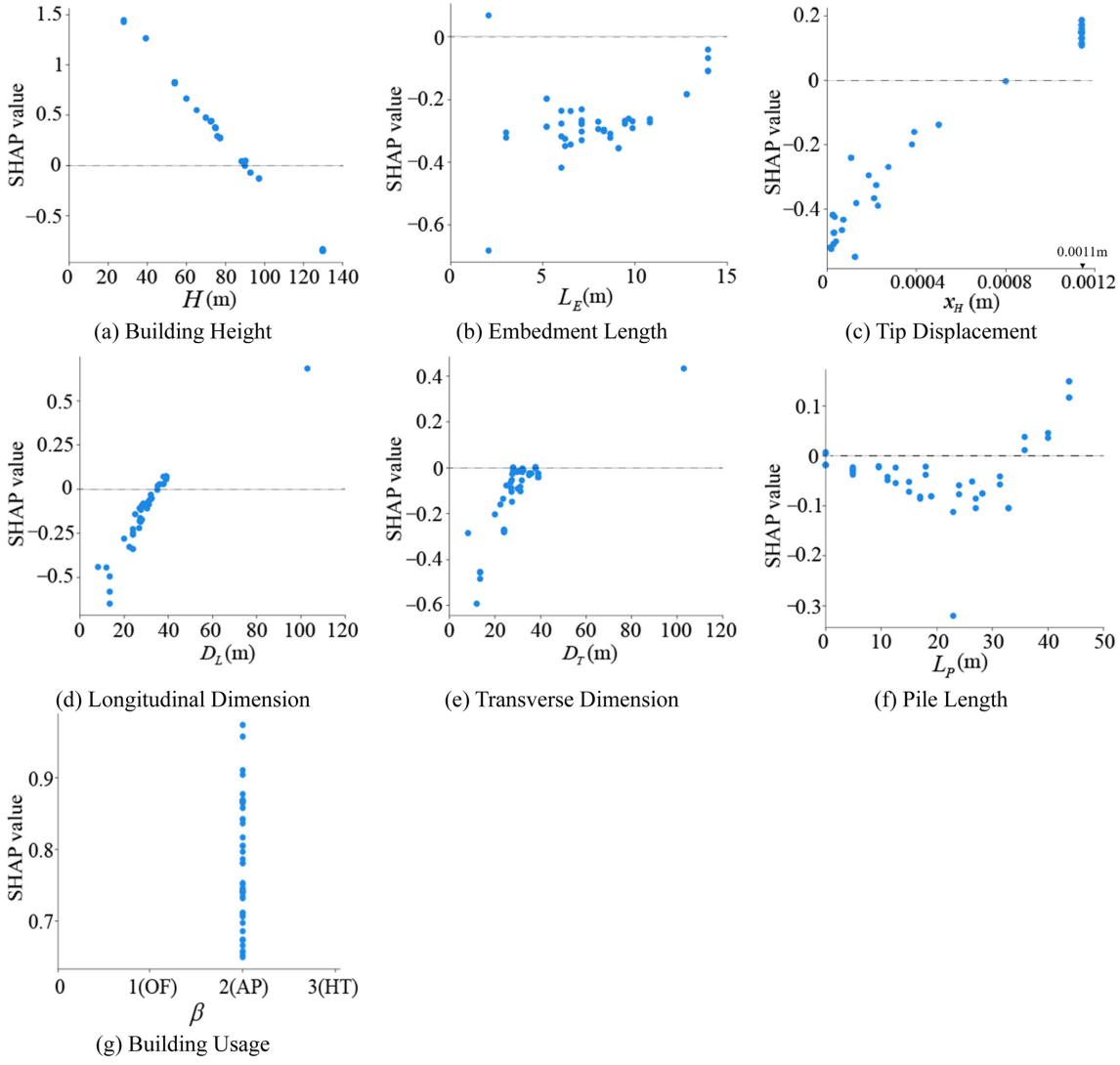


Fig. 14. Variations of SHAP values with seven parameters for damping ratios of RC buildings.

SHAP values are basically negative and show no clear correlation with embedment length up to $L_E \cong 10$ m. Then, it shows a slight positive correlation for deeper embedment lengths, like S buildings shown in Fig. 14(e). However, there are too few data to draw a clear conclusion.

(c) Tip Displacement x_H: As shown in Fig. 14(c), SHAP values show a clear positive correlation with tip displacement over the whole range of amplitudes in the figure. Thus, higher amplitudes give higher damping ratios. This is consistent with Tamura et al. (2000) and Tamura (2012). Here, as mentioned before, the tip displacement $x_H = 0.0011$ m is a value tentatively used for data without amplitude measurements in this analysis. This is the mean value of the measured amplitudes of all data including S buildings, SRC buildings and RC buildings, after removing the data without amplitude measurements. So, the plots at $x_H = 0.0011$ m should be treated as a reference.

(d) Longitudinal Dimension D_L: As shown in Fig. 14(d), SHAP values show a clear positive correlation with longitudinal dimension D_L. Thus, larger longitudinal dimensions give higher damping ratios, and this is consistent with the S buildings shown in Fig. 12(c) and the damping predictor proposed by Jeary (1986). This might be due to more significant SSI effects for larger longitudinal dimension D_L.

(e) Transverse Dimension D_T: As shown in Fig. 14(e), SHAP values show a clear positive correlation with transverse dimension D_T, in a similar manner to longitudinal dimension D_L shown in Fig. 14(d). Thus, larger transverse dimensions give higher damping ratios.

(f) Pile Length L_P: As shown in Fig. 14(f), SHAP values show a negative correlation with pile length L_P up to $L_P \cong 30$ m, suggesting that pile length plays a role as if building height is increased, while for longer pile lengths $L_P > 30$ m, SHAP values show a positive correlation with pile length L_P. This might be attributed to the increase of constraint and friction effects for deeper piles $L_P > 30$ m. This is similar to the effect of embedment lengths L_E for damping ratios of S buildings shown in Fig. 12(e).

As shown in Fig. 7(a), the height contribution significantly influences the natural frequency, while the contributions of other parameters are comparatively small. This is why the natural periods clearly increase proportionally with building height, as demonstrated by Tamura (2012). Consequently, the natural frequencies decrease as the building height increases. Conversely, as indicated in Fig. 11(a), although the height contribution is the largest factor affecting the damping ratio, the contri-butions of the other parameters, such as tip displacement, building usage, longitudinal dimension, and so on, are also comparable and not negligible. Therefore, when plotting damping ratios against building heights, there is considerable scatter because other parameters also influence the damping ratio.

5. Concluding Remarks

ML models are investigated for predicting the fundamental natural frequencies and the fundamental damping ratios of buildings based on the JDDB. The ML models give better predictions than the formulae by Tamura (2012). The correlation coefficients between the predicted natural frequencies by Eq. (1) and the measured natural frequencies (JDDB) are 0.942 (S), 0.894 (SRC), and 0.969 (RC). They are improved by the ML models as 0.963 (S), 0.924 (SRC) and 0.970 (RC). The correlation coefficients between the predicted damping ratios by Eqs. (4) and (5) and the measured JDDB damping ratios are 0.146 (S), 0.716 (RC), and they are improved by the ML models as 0.364 (S) and 0.764 (RC). The improvement is not drastic but obvious.

The most important result of this study is the evaluation of the roles of parameters affecting the dynamic properties of buildings by using the XML technique. The contribution tendency of each parameter is summarized as follows and tabulated in Table 5.

Fundamental Natural Frequency f_1: The importances of the parameters are globally in the following order: Building Height H; Material Type α; Embedment Lengths L_E; Longitudinal Dimension D_L; Building Usage β; Pile Length L_P; Transverse Dimension D_T; and the Tip Displacement x_H. The importance of Building Height H is predominant, and the other parameters' contributions are less than a quarter that of Building Height H. Especially, the contribution of Tip Displacement x_H is minimal. Therefore, it might be reasonable that the traditional formula simply gave predictions based on building height H only. The natural frequency f_1 decreases with building height H. Basically, office buildings show lower natural frequencies, and hotel buildings show higher natural frequencies. Residential apartment buildings are similar to hotel buildings but have slightly lower natural frequencies. Spread foundations give higher natural frequencies, because they are applied in deep-embedment buildings or hard soils. Natural frequency f_1 decreases with pile length L_P up to $L_P \cong 30$ m, as if the building height is increased. This tendency saturates and no more decreasing tendency is observed for $L_P > 30$ m. The natural frequency f_1 decreases with embedment lengths L_E up to $L_E \cong 10$m, as if the building height is increased, then no clear tendency is observed for $L_E > 10$ m like pile length L_P. Natural frequency f_1 increases with longitudinal dimension D_L, and this tendency is especially clear for RC buildings. Transverse dimension D_T does not show a clear tendency for the fundamental natural frequency f_1. As most of the JDDB are low-amplitude data, no dependence of natural frequency on amplitude can be observed, either.

Fundamental Damping Ratio ζ_1: The importances of the parameters are globally in the following order: Building Height H; Tip Displacement x_H; Building Usage β; Longitudinal Dimension D_L; Material Type β; Embedment

Table 5. Contribution tendency of each parameter to dynamic property of buildings

Natural Frequencies f_1				Damping Ratio ζ_1			
H (Building Height)	↘			H (Building Height)	↘		
α (Material Type)	↗			x_H (Tip Displacement)	↗	Up to x_c	−
β (Building Usage)	↗			β (Building Usage)	↗		
L_P (Pile Length)	↘	Up to 30 m	→	α (Material Type)	↗		
L_E (Embedment Length)	↘	Up to 10 m	→	D_L (Longitudinal Dimension)	↗		
D_L (Longitudinal Dimension)	↗			D_T (Transverse Dimension)	↗	(not so clear)	
D_T (Transverse Dimension)	−			L_E (Embedment Length)	↘	Up to 10m	↗
x_H (Tip Displacement)	−			L_P (Pile Length)	↗		

NOTE: Material Type: α=1 (S), 2 (SRC), 3 (RC)
Building Usage: β=1 (Offices), 2 (Residential Apartments), 3 (Hotels)
↗ : Increase with increasing parameter ↘ : Decrease with increasing parameter
→ : No change with increasing parameter − : No clear tendency
The values and x_c indicate the infection points, where x_c is the critical tip displacement (Tamura, 2012).

Length L_E; Transverse Dimension D_T; and Pile Length L_P. The contribution of building height H is largest but the other parameters' contributions to damping ratio ζ_1 are also significant. It is also understandable that the traditional formula included not only building height H but also tip displacement x_H, e.g. Tamura (2012), or longitudinal dimension D_L, e.g. Jeary (1986). It is strongly suggested that the other parameters should be included in the damping predictors. The damping ratio ζ_1 decreases with building height H, and this decreasing tendency is kept consistent up to the highest building in the JDDB without saturation. This might be attributed to decreasing SSI effects with increasing building height H. Damping ratio ζ_1 increases with tip displacement x_H, but this increasing tendency doesn't continue up to very large amplitudes. For S buildings, it stops at around $x_H/H = 3 \times 10^{-5}$, which is consistent with the critical tip drift ratio reported by Tamura (2012). Building usage β is also an important parameter. Damping ratio ζ_1 increases depending on building usage in the following order: (office buildings) < (residential apartment buildings) < (hotel buildings). This might be attributed to the friction effects of the contact surfaces of partitions and interior walls, and buildings with many partitions and interior walls show higher damping ratios ζ_1. Damping ratio ζ_1 increases with longitudinal dimension D_L, and this increasing tendency is consistent with the damping predictor by Jeary (1986). Transverse dimension D_T also plays a similar role to longitudinal dimension D_L, but this tendency is less significant. Damping ratio ζ_1 decreases with embedment length L_E up to $L_E \cong 10$ m, as if building height H is increased. However, damping ratio ζ_1 increases with embedment length L_E for larger embedment lengths $L_E >$ 10m. The spread foundation ($L_P = 0$) basically gives a lower damping ratio ζ_1. Damping ratio ζ_1 increases with pile length L_P, probably because of the more significant SSI effects.

In summary, ML models for predicting natural frequency and damping ratio are examined, and some improvements of predictions are made compared to the traditional formula. The contributions of eight parameters can be elucidated by applying XML techniques to the JDDB. Therefore, during the practical design stage, engineers can control the natural frequency and damping ratio by adjusting these parameters as much as possible. Based on this study, more useful and accurate predictors for the natural frequency and damping ratio, considering a variety of parameters, are desired to be developed. In the actual building design, the uncertainty of dynamic properties should also be taken into account, as reported by Havilland (1976). However, these uncertainties might be minimized through this type of study.

Acknowledgement

This research was partially supported by 111 Project of China (B18062, B13002), the National Natural Science Foundations of China (52221002, 52308481), and the TPU Wind Engineering Joint Usage/ Research Center Project of MEXT Japan (JPMXP0619217840). The authors are grateful for these financial supports.

Reference

AIJ Report, 2000, Damping in buildings, Architectural Institute of Japan (AIJ), Tokyo, Japan (in Japanese).

Andonie, R., 2019, Hyperparameter optimization in learning systems, *Journal of Membrane Computing*, 2019, 1, 279-91.

Aquino, R.E., Tamura, Y., 2013a, Framework for structural damping predictor models based on stick-slip mechanism for use in wind-resistant design of buildings, *Journal of Wind Engineering and Industrial Aerodynamics*, 117, 25-37.

Aquino, R.E., Tamura, Y., 2013b, On stick-slip phenomenon as primary mechanism behind structural damping in wind-resistant design applications, *Journal of Wind Engineering and Industrial Aerodynamics*, 115, 121-136.

Asteris, P.G., Repapis, C.C., Tsaris, A.K., Di Trapani, F., Cavaleri, L., 2015, Parameters affecting the fundamental period of infilled RC frame structures, *Earthquakes and Structures*, 9, 999-1028.

Asteris, P.G., Tsaris, A.K., Cavaleri, L., Repapis, C.C., Papalou, A., Di Trapani, F., Karypidis, D.F., 2016, Prediction of the fundamental period of infilled RC frame structures using artificial neural networks, Computational Intelligence and Neuroscience 2016.

Asteris, P.G., Nikoo, M., 2019, Artificial bee colony-based neural network for the prediction of the fundamental period of infilled frame structures, *Neural Computing & Applications*, 31, 4837-4847.

Boger, Z. , Guterman, H., 1997, Knowledge extraction from artificial neural network models, IEEE.

Charalampakis, A.E., Tsiatas, G.C., Kotsiantis, S.B., 2020. Machine learning and nonlinear models for the estimation of fundamental period of vibration of masonry infilled RC frame structures, Engineering Structures, 216.

Ellis, B.R., 1980, An assessment of the accuracy of predicting the fundamental natural frequencies of buildings and the implications concerning the dynamic analysis of structures, Proceedings of the Institution of Civil Engineers, Part 2 - *Research and Theory*, 69, 763-776.

Ha, T., Shin, S.-H., Kim, H., 2020, Damping and natural period evaluation of tall RC buildings using full-scale data in Korea, Applied Sciences - Basel, 10.

Havilland, R., 1976, A study of the uncertainties in the fundamental translational natural periods and damping values for real buildings, *Massachusetts Institute of Technology*, PB-253, pp.188.

Haykin SS, 2009, Neural networks and learning machines, Prentice Hall/Pearson.

Jeary, A.P., 1986, Damping in tall buildings - a mechanism and a predictor, *Earthquake Engineering & Structural Dynamics*, 14, 733-750.

Lagomarsino, S., 1993, Forecast models for damping and vibration periods of buildings, *Journal of Wind Engineering and Industrial Aerodynamics*, 48, 221-239.

Lundberg, S.M., Lee, S.I., 2017, A unified approach to interpreting model predictions, 31st Annual Conference on Neural Information Processing Systems (NIPS).

Mangalathu, S., Hwang, S.-H., Jeon, J.-S., 2020, Failure mode and effects analysis of RC members based on machine-learning-based SHapley Additive exPlanations (SHAP) approach, *Engineering Structures*, 219.

Oliveira, C.S., Navarro, M., 2010, Fundamental periods of vibration of RC buildings in Portugal from in-situ experimental and numerical techniques, *Bulletin of Earthquake Engineering*, 8, 609-642.

Ono, J., Satake, N. and Sasaki, A., 1995, Characteristics of damping in buildings based on full-scaledata (Part 2 SRC buildings & RC buildings), *Summaries of Technical Papers of Annual Meeting*, AIJ, II, 881-882. (in Japanese)

Sasaki, A., Satake, N., Arakawa, T., Suda, K., Ono, J., Morita, K., 1997, Damping properties of buildings using full-scale data, Proceedings of the Symposium on Damping Technology of the 21st Century, Dynamics and Design Conference, The Japan Society of Mechanical Engineers, Centennial Grand Congress. (in Japanese)

Satake, N., Ono, J. and Sasaki, A., 1995, Characteristics of damping in buildings based on full-scale data (Part 1 Steel buildings). Summaries of *Technical Papers of Annual Meeting*, AIJ, II, 879-880. (in Japanese)

Satake, N., Arakawa, T. and Morita, K., 1997a, Characteristics of damping in steel buildings based on full-scale data - Differences due to foundation types, measuring methods and damping evaluation techniques, Proceedings of the 67th Research Meetings. (in Japanese)

Satake, N., Arakawa, T. and Suda, K., 1997b, Damping properties of steel structure building using full-scale testing data, Part 1 Difference of damping properties by foundation types, *Summaries of Technical Papers of Annual Meeting*. (in Japanese)

Shi, W.X., Chen, X., Cao, J.L., 2013, Multi-factor predictive models of structural fundamental natural period, Engineering Mechanics.

Shioya, K., Uesu, K., Tamura, Y., Kanda, J., (1993), Dynamic characteristics of reinforced concrete high-rise apartment buildings, *Summaries of Technical Papers of Annual Meeting*, AIJ, I, 481-482. (in Japanese)

Suda, K., Satake, N., Ono, J. and Sasaki, A., 1996. Damping properties of buildings in Japan. *Journal of Wind Engineering and Industrial Aerodynamics*, 59. 383-396.

Suda, K., Satake, N. and Sasaki, A., 1997, Damping properties of steel structure building using full-scale testing data, Part2 Difference of damping properties by building uses and dimensions, *Summaries of Technical Papers of Annual Meeting*, AIJ, II, 733-734. (in Japanese)

Tamura, Y., Yamada, M., Yokota, H., 1994, Estimation of structural damping of buildings, Proceedings of Structures Congress XII, ASCE, 2, 1012-1017.

Tamura, Y. and Suganuma, S., 1996, Evaluation of amplitude-dependent damping and natural frequency of buildings during strong winds, *Journal of Wind Engineering and Industrial Aerodynamics*, 59, 115-130.

Tamura, Y., 1997, Japanese damping database, Proceedings of Structures Congress XV, *ASCE*, 2, 1064-1067.

Tamura, Y., 1998, Damping in buildings in Japan, Proceedings on CD-Rom, T193-2, Structural Engineers World Congress (SEWC), San Francisco, 8.

Tamura, Y., Suda, K., Sasaki, A., 2000, Damping in buildings for wind resistant design, 1st International Symposium on Advances in Wind and Structures (WAS-2000), Chejudo, South Korea, 115-130.

Tamura, Y., 2012, Amplitude dependency of damping in buildings and critical tip drift ratio, *International Journal of High-Rise Buildings*, 1, 1-13.

Wang, M., Yan, P., Sun, B., 2016, Review of domestic and international research for high-rise buildings' fundamental period empirical formulas, *Earthquake Engineering and Engineering Dynamics*, 36, 76-85.

Won, Y.S., 2004, Damping ratios of reinforced concrete apartment for serviceability design of wind, Journal of the Architectural Institute of Korea, *Structure & Construction*, 20, 27-34.